



HHS Public Access

Author manuscript

Chem Commun (Camb). Author manuscript; available in PMC 2021 April 30.

Published in final edited form as:

Chem Commun (Camb). 2020 April 30; 56(34): 4627–4639. doi:10.1039/d0cc01551b.

High-Resolution Probing of Early Events in Amyloid- β Aggregation Related to Alzheimer's Disease

Bikash R. Sahoo^a, Sarah J. Cox^a, Ayyalusamy Ramamoorthy^a

^a.Biophysics program, Department of Chemistry, University of Michigan, Ann Arbor, MI 48109-1055 (USA).

Abstract

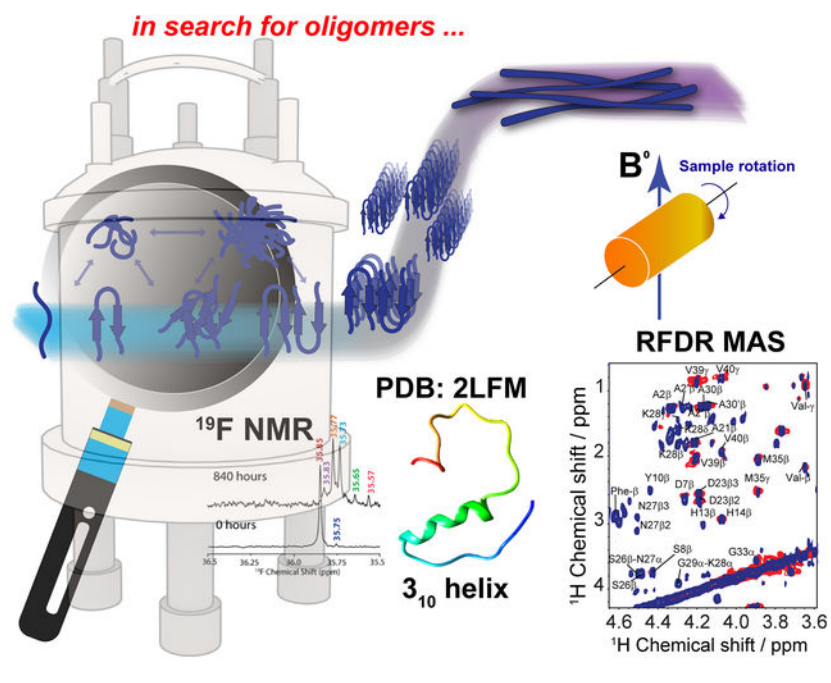
In Alzheimer's disease (AD), soluble oligomers of amyloid- β (A β) are emerging as a crucial entity in driving disease progression as compared to insoluble amyloid deposits. The lacuna in establishing the structure to function relationship for A β oligomers prevents the development of an effective treatment for AD. While the transient and heterogeneous properties of A β oligomers impose many challenges for structural investigation, an effective use of a combination of NMR techniques has successfully identified and characterized them at atomic-resolution. Here, we review the successful utilization of solution and solid-state NMR techniques to probe the aggregation and structures of small and large oligomers of A β . Biophysical studies utilizing the commonly used solution and ¹⁹F based NMR experiments to identify the formation of small size early intermediates and to obtain their structures, and dock-lock mechanism of fiber growth at atomic-resolution are discussed. In addition, the use of proton-detected magic angle spinning (MAS) solid-state NMR experiments to obtain high-resolution insights into the aggregation pathways and structures of large oligomers and other aggregates is also presented. We expect these NMR based studies to be valuable for real-time monitoring of the depletion of monomers and the formation of toxic oligomers and high-order aggregates under a variety of conditions, and to solve the high-resolution structures of small and large size oligomers for most amyloid proteins, and therefore to develop inhibitors and drugs.

Graphical Abstract

ramamoor@umich.edu.

Conflicts of interest

There are no conflicts to declare.



1. Background

1.1 Amyloid proteins and their implications in diseases

Amyloidogenic proteins are implicated in over 30 different disease states.¹ The self-assembly process, which produces highly stable beta-sheet fibers, proves to be highly conserved over many different proteins which are known to deposit as plaques in different tissues.² Diseases such as Alzheimer's disease (AD), Parkinson's, Type II Diabetes (T2D) or cataracts are specifically implicated by the misfolding and subsequent aggregation of a protein expressed in the diseased area.³ One specific protein which will be the focus of this review is Amyloid- β ($A\beta$), which is implicated as a causative factor in AD by its deposit in the extracellular space of neurons.⁴ AD is the most common form of dementia with over 5 million Americans affected by the disease, and this is expected to rise with the aging population. $A\beta$, cleaved from its Amyloid Precursor Protein (APP) by β - and γ -secretases abundantly exists with either 40 or 42 residues, each isoform with unique properties.⁵ Familial mutations in the peptide sequence creating quicker aggregating peptides, or mutations in the secretases to prefer the 42-residue length, are known to increase the risk for early onset AD.^{6,7} While much effort has been made towards the treatment of the underlying causes of AD, unfortunately, no treatments other than palliative have been approved by the FDA, which is often attributed to our lack of understanding of the structures and function of $A\beta$.

1.2 Mechanism of amyloid formation and importance of oligomers

Amyloid formation is generally thought to occur by a self-seeding mechanism in a sigmoidal fashion, in which there are three distinct steps (Figure 1).^{8,9} During the lag-phase a hydrophobic core, also known as the amyloidogenic core, can self-associate with the same sequence on another monomer via hydrophobic and aromatic π - π interactions.¹⁰

Commonly, the monomers start with a random-coil structure before self-association to form oligomers, but it is unknown what exact structures are formed during these oligomer interactions.^{11–13} Once enough of these monomers and oligomers come together, protofibrils are formed, in which the final highly ordered beta-sheet structure is obtained and then very quickly full fiber elongation takes place which is known as the nucleation phase.¹⁴ Lastly the plateau phase in which all of the monomers are depleted in solution to be fully incorporated in mature fibers. Amyloids can create fibers which can be up to microns in length, composed of many monomers aligned with a highly repetitive orientation.¹⁵ Previously formed fibers can act as seeds or a catalyst for the polymerization of fiber formation.¹⁶ Once amyloid fibers are formed, they are very stable and are highly resistant to denaturants of many types including heat, sonication, pH and some organic solvents.^{1,17}

Studies have shown that both the beginning (rich in monomers) and the end (rich in mature fibers) of this self-assembly process of amyloid aggregation can be characterized at high-resolution.¹⁸ However, the intermediate stages of aggregation in which oligomers are transiently forming and dynamically interchanging, is believed to be where the toxic species are generated in most amyloid related diseases, which elude characterization due to heterogeneity and short-lived lifetime of conformation states.^{11,19} A β peptide has also shown to form hetero-oligomers by interacting with its isoforms or other proteins.^{20–24} For A β , oligomers have been shown to be toxic in a variety of ways including membrane disruption, binding and inactivating cell surface receptors, and interactions with intracellular machinery.^{25–27} While specific oligomer preparation and isolation have been demonstrated, many of these preparations contain non-native mutations or crosslinking are off-pathway, do not form fibers, and are not lived sufficiently long enough for high-resolution structural characterization.^{11,13,25,28–32}

1.3 Experimentally following amyloid aggregation

Many biophysical techniques are commonly employed to monitor the aggregation of an amyloid peptide under various conditions.^{33,34} The commonly used thioflavin T (ThT) based fluorescent assays to monitor the kinetics of aggregation are solely based on fiber content. Circular Dichroism (CD) can monitor protein folding but the heterogeneity of oligomers can be lost and small differences can go undetected. Mass spectrometry has been instrumental in providing oligomer sizes as well as ligand binding interactions.³⁵ Atomic Force Microscopy (AFM) can provide a macroscopic view of aggregation over a range of sizes including large oligomers up to fibers in real time. While these biophysical experiments are used to obtain high-throughput information on the kinetics of aggregation and to better understand the experimental/sample conditions for further studies, obtaining atomic-resolution structural or mechanistic information of amyloid aggregation are extremely difficult using these techniques. On the other hand, transmission electron microscopy (TEM) and cryo-EM are useful in observing different fibers and their morphologies. X-ray crystallography has also been useful in the amyloid field for solving fiber and fragment fiber structures.

Nuclear magnetic resonance (NMR) is a very powerful tool for studying many facets of amyloid aggregation in both solution and solid states.^{36–42} Solution NMR is typically used for characterizing the beginning stages of amyloid formation while solid-state NMR is well

suitable for characterizing intermediates and the end stages of amyloid fiber formation (Fig. 1).^{36,41} Solution based experiments can be used for looking at monomers and low order oligomers. Monomer-monomer as well as monomer ligand interactions are commonly studied using simple two-dimensional experiments such as HSQC or HMQC in which chemical shift perturbation or line broadening observations can reveal specific individual residues' chemical environments.⁴³ NOE based 2D and 3D experiments can be used to produce three-dimensional structures of aggregates and monomers in the early stages of aggregation.⁴⁴ While solution NMR techniques are quite valuable, the large size aggregates (such as large oligomers, protofibrils and fibrils) cannot be observed due to their slow tumbling rates that result in severe line-broadening and extremely low signal-to-noise ratio.⁴⁵ On the other hand, solid-state NMR techniques have been widely used in studying high-resolution structures of fully mature amyloid fibrils as well as very large oligomers/protofibrils that are either quite stable or stabilized by freezing.^{39,46} However, detection and high-resolution probing of the formation of early oligomer intermediates and dispersion of oligomers in solution by NMR have been a challenge. This review highlights some of the recent studies to probe early events on A β aggregation using a combination of solution and solid-state NMR techniques.

2. Studying A β intermediates by solid state NMR

2.1 Effect of MAS on amyloid aggregation

One limitation in monitoring the aggregation of select amyloidogenic proteins using NMR, including A β , is the relatively slow aggregation kinetics under static conditions at low micromolar concentrations. This difficulty is typically overcome for other biophysical characterization techniques by using shaking and stirring beads.³⁵ However, these agitation methods are not possible in normal solution NMR conditions. Recent NMR studies that successfully demonstrated the feasibility of using pressure as a variable to monitor protein folding and aggregation are not covered in this review article.^{47–50} A recent study has shown a method in which A β aggregation can be accelerated and monitored in real-time using NMR spectroscopy by utilizing Magic Angle Sample (MAS) spinning.⁵¹ In this technique, the sample is loaded into a small rotor and spun at the magic angle (54.74° relative to the magnetic field axis). MAS is commonly used to obtain “solution-like” high-resolution isotropic NMR spectra of solids.

Wang et al.⁵¹ demonstrated the feasibility of using MAS experiments to induce amyloid aggregation. This mechanical rotation of the sample increases the aggregation rate so that it is more appropriate for investigation at the residue specific level by high-resolution solid-state NMR techniques (Fig. 2A), as well as to help to replicate conditions used in other biophysical assays to study amyloid proteins. Typically, under quiescent conditions a sample of A β does not show any changes in the observed proton NMR spectra over the course of 24 hours. However, spinning under 5 kHz MAS at 298 K inside the NMR probe causes the NMR peaks to decay by ~20% after 24 hours and ~50% after 72 hours. 5 kHz MAS induced substantial decay in NMR signal intensities both in aliphatic and aromatic protons highlighting mechanical rotation accelerate A β aggregation (Fig. 2A). What is so powerful about this technique is that residue specific information can be obtained as function of

amyloid aggregation. Specifically, the regions in which the aromatic vs aliphatic resonances can be detected and have been shown to decay at different rates. An interesting observation is the effect of MAS on A β aggregation is concentration dependent, but contradicts the conventional observation i.e. concentration \propto aggregation. As shown in Fig. 2B, A β under MAS aggregates faster at low concentration (15 μ M) as compared to that observed at a higher concentration (150 μ M). This study further demonstrated the feasibility of measuring the effect of amyloid inhibitors like EGCG, a polyphenolic compound found in green tea extract, which is known to generate large off-pathway oligomers of A β under MAS conditions. In this example, the decrease of aliphatic and aromatic peak intensity, and the increase of oligomer peak intensity (denoted as O1 and O2) were shown to happen very quickly (Fig. 2C,F); whereas under quiescent conditions in the presence of EGCG, no change was detected even after almost 3 days. This successful demonstration opens avenues for NMR monitoring of the residue specific aggregation information for amyloid proteins with a variety of ligands including lipids, small molecules, proteins, or other chemical tools. EGCG binding promoted the decay of A β 's aromatic proton signals under MAS that reveals the site-specific interaction that is difficult to resolve using conventional solution NMR (Fig. 2D, E). By obtaining residue specific information, mechanistic insights on early interactions of aggregation can be obtained for a better understanding on the formation of the most toxic oligomer intermediates of amyloid proteins. In addition, the experimentally measured structural constraints and molecular dynamics simulations can be used to determine high-resolution structures of the oligomers, a much-needed strategy for the development of amyloid inhibitors or chemical tools.

2.2 Transient A β oligomers are disordered like monomers

Structural polymorphism has remained as a significant feature in the amyloid cascade hypothesis and has been recently explored for mature fibers as well.^{52–55} On the other hand, for the amyloid intermediates that are characterized by toxic phenotypes, transient structural morphology and heterogeneity have led to their limited understanding.^{52,56–59} To this extent, the many classical high-resolution structure determination techniques fall short due to the inherent heterogeneous nature of A β oligomers and their growing size during aggregation. Nevertheless, several methods such as chemical crosslinking, metal binding, small-molecule binding, and protein engineering or variation in the solvent environmental condition to stabilize A β oligomers have been used.^{59–68} Even from these experiments, there exist few structural models that are proposed to be an intermediate structure of A β isolated from on-pathway aggregation.^{59,62,66,69–71,72} The formation of oligomers starting from monomers has also been reported using computational molecular dynamics simulations.^{73–77} But, the lack of a high-resolution structural model for A β oligomers isolated directly from an AD brain⁷⁸ limits the long-standing aim to correlate the existing amyloid cascade hypothesis for a successful therapeutic development against these cytotoxins. Considering the mounting evidence showing the toxic nature of amyloid intermediates, there is a need for methodological developments that are able to dig into the atomistic details of the intermediates.

Recent solid-state NMR studies have reported high-resolution structural structures/models for amyloid-fibrils including A β fibers.^{46,79–83} As a result, several polymorphic atomic-

resolution structures of A β fibers and very large oligomers/protofibrils are now available in Biological Magnetic Resonance Bank (BMRB) and Protein Data Bank (PDB).⁷⁹ Other techniques such as X-ray diffractions, small angle X-ray scattering (SAXS) and cryo-EM have also successfully delivered atomic-resolution structural information for A β fibrils and oligomers.^{62,63,84–87} However, the advances in solid-state NMR spectroscopy in studying biological solids in a heterogeneous sample environment attract further attention as a mean to look into amyloid oligomers at real-time during their on-pathway amyloid aggregation. The isolation of transient oligomers is hindered by sample preparation and purification techniques that subject the oligomers to pass via harsh conditions which could affect the morphology and are beyond the experimental control.^{88–90} For example, a 56-kDa soluble A β oligomer species has been isolated from an AD mouse brain and purified using immunoaffinity chromatography and size-exclusion chromatography (SEC).⁹¹ Similarly, small size A β oligomers (such as dimers and trimers) have been isolated directly from AD brains or naturally secreted by cultured cells have been purified using electrophoresis and chromatography methods, and have also been shown to be toxic.^{92,93} Remarkably, a study by Yang et al.⁷⁸ showed the size dependent toxic characteristics of soluble A β oligomers. This study isolated high-molecular weight A β oligomers using non-denaturing SEC that have been found to be non-toxic or slightly toxic. Interestingly, alkaline medium treatment of these A β oligomers led the dissociation and formation of low-molecular weight oligomers that were found to be cytotoxic.⁷⁸

Coupled with NMR, atomistic simulations also have been a useful technique in revealing the structural and dynamical information of A β intermediates at atomic-resolution. It is difficult to obtain a high-resolution 3D structure of A β intermediates using a single technique like NMR. This is mainly due to the limitations in obtaining a sufficient number of distance constraints to obtain a 3D structure. For example, a recent study succeeded in providing a unique β -strand structure for hIAPP (human islet amyloid polypeptide) trapped by lipid-membrane nanodiscs.⁴⁴ Such structural characterization required integration of NMR distance constraints, *ab-initio* modelling and molecular dynamics (MD) simulations to generate a 3D structure. In absence of NMR derived distance constraints, MD simulations have been proven to be useful in retrieving intermediate structural and dynamical information and the fiber elongation for several amyloidogenic proteins at atomic-resolution.^{94–96} Such structural and dynamic information have been reported for A β species such as monomer, dimer, trimer, tetramer, pentamer, and hexamer.^{73,95,97–102}

Here, we review the high-resolution structural details of A β oligomers that coexist with fibers, or filtered without rigorous purification techniques (no additives), using MAS solid-state NMR techniques.¹⁰³ Previously, solid-state NMR methods demonstrated the use of MAS-induced sedimentation that act as an ultracentrifuge to separate A β monomers from oligomers.¹⁰⁴ The aggregation of A β has been known to form a polymorphic and a heterogeneous sample mixture that includes reversible and irreversible formation of oligomeric and fibrillary aggregates; aggregate from monomers depending on the solvent, pH, temperature and concentration.¹⁰⁵ When incubating monomers over several days with or without shaking, A β typically forms heterogeneous fibrils along with globular oligomers.^{45,59,103} As reported, the A β oligomers coexist with fibers (Fig. 3) when incubated at low⁵⁹ or high concentration¹⁰³ (2E-5 mg/mL or 1mg/mL). The oligomers can be separated from

monomers and share a spherical morphology (Fig. 3A). Further, the stability of these oligomers provides a conceivable platform for the application of NMR experiments to retrieve high-resolution structural insights (Fig. 3C–E). However, the abundance of these oligomers is too small ($\approx 7\text{--}10\%$) for detection and increasing the sample concentration for NMR studies is quite challenging.¹⁰³ Another limitation for structural characterization of these low populated oligomers is the use of NMR sensitive isotope labelling ($^{15}\text{N}/^{13}\text{C}/^{19}\text{F}$). In this context, proton-detected NMR measurements highlighting the high-resolution structural details are remarkably important. Application of such cost-effective methods with dipolar recoupling MAS experiments, such as the radio frequency driven dipolar recoupling (RFDR), enabled the acquisition of 2D homonuclear $^1\text{H}/^1\text{H}$ correlation spectra (Figs. 3 and 4).¹⁰⁶ As demonstrated, these experiments do not detect signals from amyloid fibers as the sample spinning speed is not very fast enough to suppress the very large $^1\text{H}\text{--}^1\text{H}$ dipolar couplings present in fibers. On the other hand, since the dipolar couplings among protons in monomers are averaged out by their fast tumbling, their signals are suppressed by the dipolar recoupling. Thus, the RFDR based 2D NMR experiments successfully distinguished the low abundant oligomers from monomers and fibers that are otherwise not amenable for solution or other solid-state NMR characterization (Figs. 3 and 4). The detection of these oligomers is limited by conventional heteronuclear NMR techniques. For example, as shown in Fig. 4D, 2D $^1\text{H}/^{15}\text{N}$ HSQC presents a well dispersed NMR spectrum for A β monomers, but fails to provide substantial detectable residue information to probe the oligomers. In addition, although homonuclear ($^1\text{H}/^1\text{H}$) solution NMR experiments such as TOCSY and NOESY can provide atomic correlation, these atomistic information are greatly sacrificed due to line-broadening (Fig. 4).¹⁰³ The NMR spectrum of isolated oligomers differs substantially from that of monomers, but interestingly share a disordered conformation as revealed by CD spectroscopy (Fig. 3B).

2.3 Why do we care about on-pathway A β oligomers?

While experimental characterization of transient oligomeric structures of A β at atomic-resolution is tedious, their globular morphology can be easily distinguished from protofibrils or matured fibers. A study using SAXS showed the formation of cylindrical or ellipsoidal shaped A β protofibrils or oligomers induced by copper ions.⁶³ Similarly, Rezaei-Ghaleh et al.¹⁰⁷ proposed that zinc binding to N-terminus of A β induces off-pathway amorphous like aggregates using NMR. Unlike off-pathway oligomers, on-pathway oligomers have been shown to share a disordered conformation that resembles monomers and can grow in size over time (Figs. 4A–C). While off-pathway oligomers can be highly stable and vary in structural heterogeneity, pathological phenotype and size, on-pathway oligomers grow in size and can serve as seeds to nucleate the self-assembling seeding reaction. Thus, therapeutic development has often concentrated on restricting this aggregation pathway of A β to generate non-toxic species.¹⁰⁸ The design of therapeutics is highly dependent on the chemical properties of the A β surface that are significantly different for disordered monomers and oligomers. As an example, solid-state NMR studies have identified inter-residue contacts between aliphatic and alpha protons of K28-G29, S26-N27, H13-G38, and S8-E11 in on-pathway oligomers that are absent in A β monomers (Fig. 3C–E). Such inter-residue interactions restrict the degrees of freedom of side-chains in oligomers, and therefore could hinder the potential binding of designed inhibitors screened using A β monomers. In

this context, an argument can be made for looking into the role of a potent A β inhibitor, EGCG that significantly reduces A β 's neurotoxicity when treated with monomers. In contrary, metal-bound A β species (oligomers) treated with EGCG exhibited a relatively low rescuing of neurotoxicity indicating EGCG's preferential binding to A β monomers.¹⁰⁹ Thus, our understanding of A β oligomer structures derived from on-pathway aggregation not only help in understanding the aggregation pathways, but also provide substantial atomistic insights to optimize an array of currently available anti-amyloidogenic inhibitors.

3. Studying A β intermediates by solution NMR

3.1 Structure of a small molecular weight A β intermediate

As discussed above, traditional solution NMR spectroscopy, relying on NOE based distance constraints obtained from NOESY experiments, has limitations on providing structural details for high molecular weight oligomers (\approx 100 kDa). On the other hand, a lowly populated early on-pathway intermediate of A β peptide, distinct from a disordered monomer, was detected and its high-resolution three-dimensional structure has been determined using NOE constraints measured from solution NMR experiments. Traditional 2D $^1\text{H}/^1\text{H}$ NOESY and TOCSY experiments were used to resolve a partially folded A β (1–40) intermediate characterized by a 3_{10} helix spanning the central hydrophobic regions H13 to D23 (Fig. 5A,B).⁶⁹ While uniform labelling for structure determination is expensive, these traditional methods not only provide high-resolution structural insights, but also able to isolate an early intermediate structure of A β that is difficult to probe using solid-state NMR as described in section 2.2. The 3_{10} helix folding of A β (1–40) intermediate served as an important feature for A β 's aggregation and β -sheet formation. The 3_{10} helix satisfies an intermediate conformation during $\alpha \rightarrow \beta$ folding that triggers the transition of a compressed α -helix to an extended β -sheet needed for amyloid formation. Such structural transitions facilitated by a 3_{10} helix is also identified in a water-soluble amphipathic short peptide that forms amyloid.¹¹⁰ This study demonstrated the feasibility of solving the structure of lowly populated very early intermediate amyloid-beta peptide. This is in contrast to perturbative methods for stabilizing such helical intermediates (Fig. 5C) on a time-scale desired for solution NMR monitoring; non-perturbative methods like optimization of sample temperature is very useful as it traps the intermediate structures during the on-pathway peptide aggregation as shown in Figure 5C. Another solution NMR study reported an alpha-helical conformation of A β (1–40) and its destabilization by the oxidation of Met35, which is also shown to restrict β -sheet structural transition.¹¹¹ Computational simulations also identify differently populated species of A β (1–40) monomers. Zheng et al.¹¹² showed two distinguished structures for A β (1–40) that includes a major disordered structure with a short-helix in the central hydrophobic core and a β -hairpin structure between the central hydrophobic core and A30-V36 from MD simulation. Notably, the MD simulation at 300 K showed that A β (1–40) favors mostly a stable helical conformation as compared to an unstable β -hairpin structure, which becomes prominent and increasingly stable when A β (1–40) forms an oligomer. Similarly, another MD simulation study identified a transient 3_{10} helix in A β (1–42) by varying the ionic strength.¹¹³ Thus, non-physiological conditions such as low temperature sample preparation can stabilize the early intermediates of A β (1–40) and

could provide high-resolution structural characterization for A β (1–40) intermediates (Fig. 5C).

3.2 Real time monitoring the formation of A β intermediates by ^{19}F NMR

In addition to sample heterogeneity and interconversion among amyloid intermediates, spectral overlapping has been an obstacle for obtaining high-resolution structural information from NMR experiments. The structure elucidation using solution NMR greatly relies on the sequential assignment and backbone connectivity that are often limited by the signal overlapping and line-broadening (in both 1D and 2D NMR measurements) especially when the size of the targeted molecule grows. To this extent, development of alternative solution NMR methods apart from the traditional homonuclear (TOCSY/NOESY) NMR experiments would be useful in studying amyloid intermediates growing on-pathway during aggregation. As an example, solution ^{19}F NMR offers an ideal alternative¹¹⁴ to probe amyloid intermediates as fluorine serves as an extremely rare nucleus that does not interfere with other NMR active nuclei such as $^1\text{H}/^{15}\text{N}/^{13}\text{C}$ in biological samples. The sensitivity of ^{19}F chemical environment during the conformational alteration in amyloids following the fibrillation pathway can be selectively correlated even for a small change in the ^{19}F chemical shifts. Moreover, for amyloids a key feature is their aggregation propensity that relies on the initial concentration. That said, early oligomers are expected when the A β peptide samples are prepared at high concentration. To this extent, ^{19}F NMR is useful as compared to ^1H NMR as it renders a single distinct peak (Fig. 6A).¹¹⁵ Like ^1H NMR, ^{19}F NMR spectra can be compared considering two different factors to discriminate oligomers from non-aggregated samples¹¹⁵ that include chemical shift changes and line-broadening (in oligomers) measured by acquiring NMR spectra as a function of time (Fig. 6B). Similarly, ^{19}F NMR include limitations in resolving the peaks for large species such as protofibrils, but could able to resolve low molecular weight intermediates of different size at high-resolution with distinct spectral peaks separated by tens of Hz (Fig. 6B).¹¹⁵

4. Mapping local ordered and disordered regions in non-aggregated A β docked with aggregated species

Besides the effort in characterizing the high-resolution structure of A β intermediates as discussed above, understanding their molecular mechanism in proceeding the fibrillation is important. This molecular process involves generation of intermediates during the seeding reaction where a monomer docks with preformed fibers. As discussed in section 2.2 (Fig. 4), on-pathway intermediates are important target that grow in size (Fig. 4A–C) and proceed the self-assembly process to yield metastable fibers and identification of such molecular processes at atomic level is important. Thus, a breakthrough for therapeutic advancement urges the need for real time mapping of residues specific binding interface during the course of the seeding reaction that generates intermediate species. Realization of this goal requires both local and global structural information for long-time spans and with shorter time intervals of experimental measurements. Although, this is one of the most challenging tasks that remains unexplored and experimentally daunting, a recent study used NMR experiments to obtain such mechanistic insights (Fig. 7).¹¹⁶

Solution NMR experiments, such as Band-Selective Optimized Flip Angle Short Transient-Heteronuclear Multiple Quantum Correlation (SOFAST-HMQC), make it feasible to retrieve both local and global folding information during a seeding reaction. Using SOFAST-HMQC¹¹⁷, the structural and binding site information were obtained through mapping the regions of monomers interacting with seeded fibers in a solution sample by periodically monitoring the A β backbone ¹H/¹⁵N resonances. The fast 2D NMR data acquisition (typically in minutes) makes it feasible to plot residue specific mapping as A β monomers dock to matured or sonicated short fibers (Fig. 7A). The results reported in this study extended our current understanding of transient association steps involved in the fibrillation at atomic level. For example, residue specific NMR parameters measured from SOFAST-HMQC experiments as a function of aggregation time revealed a substantial difference between A β monomer binding to protofibers and fibers due a significant difference in the surface of the large supramolecular structure. While the amyloidogenic segment in A β , comprised of sequence ₁₆KLVFFA₂₁, preferentially binds to protofibers⁴⁰, Brender et al.¹¹⁶ showed the central domain spanning residues 19–27 prefer binding to fully matured A β fibers (Fig. 7B, C). An important and interesting observation in this study is the identification of new oligomer species that generate and coexist with the fully matured fibers (Fig. 7D). Several new minor peaks were identified in the vicinity of C-terminal residues such as G33 and V40 when A β monomers are docked with matured or sonicated fibers. This study proposed that the appearance of these new peaks could be from the new oligomers that are generated at the fiber end. Moreover, their findings also provide mechanistic insight to underlining the secondary nucleation process during the seeding reaction. Overall, this study sheds light on the importance of determining the differential binding modes of A β monomers to aggregated species that are not monomorphic. The slight shift in the binding interface could provide additional insights for the design of peptide inhibitors as reported by Brender et al.¹¹⁶ A peptoid inhibitor designed from A β sequence (30–34) AIAL was shown to inhibit A β fibrillation by selectively binding to the hydrophobic region ₁₇LVFFA₂₁.¹¹⁸ An optimal binding sequence is needed to design successful peptide inhibitors in order to arrest the fibrillation, as the targeted sequence motif ‘KLVFF’ binding to protofibers showed a moderate effect on suppressing fiber elongation and toxicity.^{119,120} An octapeptide derived from activity dependent neuroprotective protein has been shown to form amyloid fibers, but capable of inhibiting A β fibrillation. This highlights a competitive seeding reaction can be achieved to suppress self-assembled A β aggregates.¹²¹ Thus, a successful therapeutic development for AD requires the identification and mapping of an optimal local domain of A β that dock to on-pathway aggregates to proceed the seeding reaction homogeneously or cross-seed to less toxic fibrillogenic peptide segments. In this direction, computational simulations also have demonstrated a dock-lock mechanism in which docking of a disordered monomer to an oligomer/fiber induce a structural rearrangement (form β -structure) following the elongation/growth of the complex.⁹⁶

5. Limitations of NMR techniques and alternative approaches

As discussed in the previous sections, both solution and solid-state NMR are able to track the transient and heterogeneous species of A β providing atomic-resolution details. Nevertheless, a major limitation of these NMR techniques is the elucidation of a 3D

structural model due to the lack of sufficient distance restraints as shown in Figs. 2, 3 and 4. In addition, the driving molecular forces that govern structural transitions and oligomerization are difficult to probe using NMR. These limitations require involvement of other approaches to build structural models of A β oligomer for the design of drug/inhibitor. MD simulations, as briefly discussed in section 2.2, can be used in combination with NMR to obtain structural models. We refer the readers to the published review articles on MD simulation studies.^{122,123} All-atom MD simulations provide insights into structural transition on a time-scale of picoseconds to microseconds. MD simulation has been shown that electrostatic interactions are the major source for the structural fluctuation and stability in A β peptides when compared to the wild-type A β _{10–35} with its Dutch mutant (E22Q).¹²⁴ The simulations probed the early events of structural transition where the E22Q mutant was found to be more flexible as compared to the wild-type and adopts predominantly α -helical conformation that is in line with experimental observations. The MD simulation predicted conformational changes in the Dutch mutant could be due to an increase in the hydrophobic solvation resulting in an enhancement of desolvation and aggregation propensity as compared to the wild-type A β peptide.⁹⁸ As discussed in Section 3, identification and characterization of early amyloid intermediates are of significant importance to better understand the mechanism of amyloid aggregation and the formation of toxic intermediates. In studying this, it was proposed that hydrophobic interactions between monomers primarily stabilize A β _{10–35} dimers and the peptide molecules experience a substantial conformational change during dimerization.⁹⁷ By comparing two dimer models (which are mentioned as \mathcal{E} -dimer and ϕ -dimer) differing in their monomer packing, they revealed that the \mathcal{E} -dimer stabilized by electrostatic interaction is energetically less stable as compared to the ϕ -dimer that is stabilized by hydrophobic interactions. These results revealed a differential energy landscape preceding nucleation, which is mostly due to peptide-peptide and peptide-water interactions. Such information are not easy to obtain from NMR. MD simulation has also been successful in generating an array of different planar β -strand dimer conformations for A β (1–40) and A β (1–42).⁷⁶ Another simulation study identified significantly more number of dimers in A β (1–40), whereas A β (1–42) has been shown to generate pentamers which correlates to the difference in the aggregation propensities of these two isoforms.¹²⁵

Following the discussion in Section 4, MD simulation has been successful in establishing a model to explain the dock-lock mechanism during a seeding reaction.⁹⁴ Massi et al. proposed two different pathways for the deposition of A β or its mutants that includes a fast deposition through nucleation and deposition of A β to pre-existing fibers undergoing structural reorganization. Using microseconds all-atom MD simulations, Nguyen et al. showed the docking of A β monomers to water-soluble oligomers.⁹⁵ The simulation results showed that the trimers of an A β fragment (16–22), with an anti-parallel structure, undergo structural reorganization and on a time scale of hundreds of nanoseconds when added with monomers; the trimers are shown to grow in size to form tetramers, pentamers and hexamers with a relatively more ordered (β -sheet) conformation.⁹⁵ The added monomer was observed to follow a two-step mechanism where it first docks to the anti-parallel trimer leading to an extension of the chain followed by a substantial change in its conformation with a growing β -sheet content.⁹⁵

Recent advancement in electron paramagnetic resonance (EPR) spectroscopy provides structural insights into A β oligomers. Using site-directed spin-labelling, Gu et al. showed a site-specific mobility and rigidity in A β oligomer. The order of rigidity increases from N- to C-terminus with the residues 29–40 tightly packed.¹²⁶ A monomer unit in the model structure of A β (1–42) oligomers, built using EPR distance restraints, is comprised of three anti-parallel β -strands forming a single β -sheet.¹²⁷ While such structural information is difficult to obtain using solution NMR, solid-state NMR is capable of providing these information but at the cost of relatively a large amount of sample and residue specific selective isotope labelling.^{128,129} X-ray crystallography shown to be an alternative method in resolving A β oligomers; however require peptide chemical modifications for crystallization. Using chemically modified A β mimetic peptides, Nowick et al. reported A β trimer, hexamer and dodecamer structures.^{61,130} The tight packing of C-terminal residues influencing oligomer formation correlate to NMR observation that identified several inter-residue cross-peaks (K28-G29, S26-N27, H13-G38 and S8-E11) in the 2D RFDR measurement suggesting their involvement in the oligomer formation (Fig. 3). Nevertheless, mutagenesis analysis further suggested that the C-terminal hydrophobic residues (I31, I32, L34, V39, V40, and I41) are key determinants of A β oligomerization.¹³¹ RFDR experiments also indicated the important involvement of serine and glycine fingerprint regions influencing the formation of disordered oligomers. Taken together, the suggested regions are potential target sites for designing inhibitors to suppress A β toxicity.^{132,133}

6. Concluding Remarks

Although obtaining atomic-resolution structural details of A β intermediate species continues to be a major challenge, a combination of solution and solid-state NMR techniques and MD simulations can be used to overcome some of these challenges. As described in this review article, recent studies have successfully developed 3D structural models of amyloid intermediates transitioning from a disordered state to partially folded state. Of particular interest, these structural models established a platform for both experimental and computational biophysicists to develop or optimize anti-amyloidogenic inhibitors. However, bridging the structural gap between disordered and ordered (β -sheet rich) states of A β requires further attention and methodological advancements where NMR is a promising technique. In addition, the recent advancement of cryo-EM in picturing molecules of several hundred kDa further brings hope to visualize atomic resolution of A β globular oligomers. In parallel, the recent advances in hardware such as very fast MAS, MAS CryoProbe¹³⁴ and sub-milligram sample rotors etc. could enable high throughput structural studies of A β oligomers in the near future.

Acknowledgements

A. R. acknowledge funding from the National Institutes of Health (AG048934). We thank Dr. John Staub and Dr. Devarajan Thirumalai for fruitful discussions. A.R. also thanks Dr. Jeffrey Brender (NIH) for the valuable contributions to the amyloid research in the lab.

References

1. Harrison RS, Sharpe PC, Singh Y and Fairlie DP, *Rev. Physiol. Biochem. Pharmacol*, 2007, 159, 1–77. [PubMed: 17846922]
2. Chiti F and Dobson CM, *Annu. Rev. Biochem*, 2006, 75, 333–366. [PubMed: 16756495]
3. Knowles TPJ, Vendruscolo M and Dobson CM, *Nat. Rev. Mol. Cell Biol*, 2014, 15, 384–396. [PubMed: 24854788]
4. Hamley IW, *Chem. Rev*, 2012, 112, 5147–92. [PubMed: 22813427]
5. O'Brien RJ and Wong PC, *Annu. Rev. Neurosci*, 2011, 34, 185–204. [PubMed: 21456963]
6. DeToma AS, Salamekh S, Ramamoorthy A and Lim MH, *Chem. Soc. Rev*, 2012, 41, 608–621. [PubMed: 21818468]
7. Ono K, Condrón MM and Teplow DB, *J. Biol. Chem*, 2010, 285, 23186–23197. [PubMed: 20452980]
8. Morris AM, Watzky MA and Finke RG, *BBA - Proteins Proteomics*, 2008, 1794, 375–397. [PubMed: 19071235]
9. Meisl G, Kirkegaard JB, Arosio P, Michaels TCT, Vendruscolo M, Dobson CM, Linse S and Knowles TPJ, *Nat. Protoc*, 2016, 11, 252–272. [PubMed: 26741409]
10. Cohen SIA, Vendruscolo M, Dobson CM and Knowles TPJ, *J. Mol. Biol*, 2012, 421, 160–171. [PubMed: 22406275]
11. Nagel-Steger L, Owen MC and Strodel B, *ChemBioChem*, 2016, 17, 657–676. [PubMed: 26910367]
12. Young LM, Tu LH, Raleigh DP, Ashcroft AE and Radford SE, *Chem. Sci*, 2017, 8, 5030–5040. [PubMed: 28970890]
13. Breydo L, Kurouski D, Rasool S, Milton S, Wu JW, Uversky VN, Lednev IK and Glabe CG, *Biochem. Biophys. Res. Commun*, 2016, 477, 700–705. [PubMed: 27363332]
14. Algamal M, Ahmed R, Jafari N, Ahsan B, Ortega J and Melacini G, *J. Biol. Chem*, 2017, 292, 17158–17168. [PubMed: 28798235]
15. Riek R, *Cold Spring Harb. Perspect. Biol*, 2017, 9, a023572. [PubMed: 27793967]
16. Ruschak AM and Miranker AD, *Proc. Natl. Acad. Sci*, 2007, 104, 12341–12346. [PubMed: 17640888]
17. Chuang E, Hori AM, Hesketh CD and Shorter J, *J. Cell Sci*, 2018, 131, 131.
18. Chiti F and Dobson CM, *Annu. Rev. Biochem*, 2017, 86, 27–68. [PubMed: 28498720]
19. Benilova I, Karran E and De Strooper B, *Nat. Neurosci*, 2012, 15, 349–357. [PubMed: 22286176]
20. Baldassarre M, Baronio CM, Morozova-Roche LA and Barth A, *Chem. Sci*, 2017, 8, 8247–8254. [PubMed: 29568473]
21. Ly S, Altman R, Petrlova J, Lin Y, Hilt S, Huser T, Laurence TA and Voss JC, *J. Biol. Chem*, 2013, 288, 11628–11635. [PubMed: 23430745]
22. Mouchard A, Boutonnet MC, Mazzocco C, Biendon N and Macrez N, *Sci. Rep*, 2019, 9, 3989. [PubMed: 30850702]
23. Muñoz SS, Garner B and Ooi L, *Neurochem. Res*, 2018, 0, 0.
24. Sahoo BR, Bekier ME, Liu Z, Kocman V, Stoddard AK, Anantharamaiah GM, Nowick J, Fierke CA, Wang Y and Ramamoorthy A, *J. Mol. Biol*, 2020, 432, 1020–1034.
25. Cavallucci V, D'Amelio M and Cecconi F, *Mol. Neurobiol*, 2012, 45, 366–378. [PubMed: 22415442]
26. Zhao LN, Long H, Mu Y and Chew LY, *Int. J. Mol. Sci*, 2012, 13, 7303–7327. [PubMed: 22837695]
27. Sahoo BR, Genjo T, Cox SJ, Stoddard AK, Anantharamaiah GM, Fierke C and Ramamoorthy A, *J. Mol. Biol*, 2018, 430, 4230–4244. [PubMed: 30170005]
28. Hayden EY, Conovaloff JL, Mason A, Bitan G and Teplow DB, *Anal. Biochem*, 2016, 518, 78–85. [PubMed: 27810329]

29. Querol-Vilaseca M, Colom-Cadena M, Pegueroles J, Nuñez-Llaves R, Luque-Cabecerans J, Muñoz-Llahuna L, Andilla J, Belbin O, Spires-Jones TL, Gelpi E, Clarimon J, Loza-Alvarez P, Fortea J and Lleó A, *Sci. Rep.*, 2019, 9, 5181. [PubMed: 30914681]
30. Jang H, Zheng J, Lal R and Nussinov R, *Trends Biochem. Sci.*, 2008, 33, 91–100. [PubMed: 18182298]
31. Riek R and Eisenberg DS, *Nature*, 2016, 539, 227–235. [PubMed: 27830791]
32. Ehrnhoefer DE, Bieschke J, Boeddrich A, Herbst M, Masino L, Lurz R, Engemann S, Pastore A and Wanker EE, *Nat. Struct. Mol. Biol.*, 2008, 15, 558–566. [PubMed: 18511942]
33. Nilsson BL and Doran Editors TM, *Peptide Self-Assembly*, Springer New York, New York, NY, 2018, vol. 1777.
34. Iadanza MG, Jackson MP, Hewitt EW, Ranson NA and Radford SE, *Nat. Rev. Mol. Cell Biol.*, 2018, 19, 755–773. [PubMed: 30237470]
35. Abdolvahabi A, Shi Y, Rasouli S, Croom CM, Chuprin A and Shaw BF, *Biophys. J.*, 2017, 112, 250–264. [PubMed: 28122213]
36. Karamanos TK, Kalverda AP, Thompson GS and Radford SE, *Prog. Nucl. Magn. Reson. Spectrosc.*, 2015, 88–89, 86–104.
37. Kovermann Michael, Rogne Per and Wolf-Watz Magnus, *Q. Rev. Biophys.*, 2016, 49, e6. [PubMed: 27088887]
38. Mishra R, Geyer M and Winter R, *ChemBioChem*, 2009, 10, 1769–1772. [PubMed: 19575373]
39. Meier BH, Riek R and Böckmann A, *Trends Biochem. Sci.*, 2017, 42, 777–787. [PubMed: 28916413]
40. Fawzi NL, Ying J, Ghirlando R, Torchia DA and Clore GM, *Nature*, 2011, 480, 268–272. [PubMed: 22037310]
41. Sarkar B, Mithu VS, Chandra B, Mandal A, Chandrakesan M, Bhowmik D, Madhu PK and Maiti S, *Angew. Chemie - Int. Ed.*, 2014, 53, 6888–6892.
42. Ahmed R and Melacini G, *Chem Commun*, 2018, 54, 4644–4652.
43. Schleucher J, Schwendinger M, Sattler M, Schmidt P, Schedletzky O, Glaser SJ, Sorensen OW and Griesinger C, *A general enhancement scheme in heteronuclear multidimensional NMR employing pulsed field gradients*, 1994, vol. 4.
44. Rodriguez Camargo DC, Korshavn KJ, Jussupow A, Raltchev K, Goricanec D, Fleisch M, Sarkar R, Xue K, Aichler M, Mettenleiter G, Walch AK, Camilloni C, Hagn F, Reif B and Ramamoorthy A, *Elife*, 2017, 6, e31226. [PubMed: 29148426]
45. Sahoo BR, Genjo T, Nakayama TW, Stoddard AK, Ando T, Yasuhara K, Fierke CA and Ramamoorthy A, *Chem. Sci.*, 2019, 10, 3976–3986. [PubMed: 31015938]
46. Tycko R, *Annu. Rev. Phys. Chem.*, 2011, 62, 279–299. [PubMed: 21219138]
47. Silva JL, Foguel D and Royer CA, *Trends Biochem. Sci.*, 2001, 26, 612–618. [PubMed: 11590014]
48. Erlach MB, Kalbitzer HR, Winter R and Kremer W, *ChemistrySelect*, 2016, 1, 3239–3243.
49. Rosenman DJ, Clemente N, Ali M, García AE and Wang C, *Chem. Commun*, 2018, 54, 4609–4612.
50. Munte CE, Beck-Erlach M, Kremer W, Koehler J and Kalbitzer HR, *Angew. Chemie - Int. Ed.*, 2013, 52, 8943–8947.
51. Wang J, Yamamoto T, Bai J, Cox SJ, Korshavn KJ, Monette M and Ramamoorthy A, *Chem. Commun*, 2018, 54, 2000–2003.
52. Antzutkin ON, in *Modern Magnetic Resonance*, 2018, pp. 333–347.
53. Landau M, Eisenberg D, Flot D, Laganowsky A, Zhao M, Sawaya MR, Cascio D, Goldschmidt L, Soriaga AB and Colletier J-P, *Proc. Natl. Acad. Sci.*, 2011, 108, 16938–16943. [PubMed: 21949245]
54. Rasmussen J, Mahler J, Beschorner N, Kaeser SA, Häsler LM, Baumann F, Nyström S, Portelius E, Blennow K, Lashley T, Fox NC, Sepulveda-Falla D, Glatzel M, Oblak AL, Ghetti B, Nilsson KPR, Hammarström P, Staufienbiel M, Walker LC and Jucker M, *Proc. Natl. Acad. Sci.*, 2017, 114, 13018–13023. [PubMed: 29158413]
55. Tycko R, *Neuron*, 2015, 86, 632–645. [PubMed: 25950632]

56. Pham JD, Demeler B and Nowick JS, *J. Am. Chem. Soc.*, 2014, 136, 5432–5442. [PubMed: 24669785]
57. Lee SJC, Nam E, Lee HJ, Savelieff MG and Lim MH, *Chem. Soc. Rev.*, 2017, 46, 310–323. [PubMed: 27878186]
58. Sengupta U, Nilson AN and Kayed R, *EBioMedicine*, 2016, 6, 42–49. [PubMed: 27211547]
59. Sahoo BR, Genjo T, Bekier M, Cox SJ, Stoddard AK, Ivanova M, Yasuhara K, Fierke CA, Wang Y and Ramamoorthy A, *Chem. Commun. (Camb)*, 2018, 54, 12883–12886. [PubMed: 30379172]
60. Irie Y, Murakami K, Hanaki M, Hanaki Y, Suzuki T, Monobe Y, Takai T, Akagi KI, Kawase T, Hirose K and Irie K, *ACS Chem. Neurosci.*, 2017, 8, 807–816. [PubMed: 28026168]
61. Kreutzer AG and Nowick JS, *Acc. Chem. Res.*, 2018, 51, 706–718. [PubMed: 29508987]
62. Stroud JC, Liu C, Teng PK and Eisenberg D, *Proc. Natl. Acad. Sci.*, 2012, 109, 7717–7722. [PubMed: 22547798]
63. Ryan TM, Kirby N, Mertens HDT, Roberts B, Barnham KJ, Cappai R, Pham CLL, Masters CL and Curtain CC, *Metalomics*, 2015, 7, 536–543. [PubMed: 25687761]
64. Miller Y, Ma B and Nussinov R, *Proc. Natl. Acad. Sci.*, 2010, 107, 9490–9495. [PubMed: 20448202]
65. Ryan TM, Roberts BR, McColl G, Hare DJ, Doble PA, Li Q-X, Lind M, Roberts AM, Mertens HDT, Kirby N, Pham CLL, Hinds MG, Adlard PA, Barnham KJ, Curtain CC and Masters CL, *J. Neurosci.*, 2015, 35, 2871–2884. [PubMed: 25698727]
66. Wang J, Yamamoto T, Bai J, Cox SJ, Korshavn KJ, Monette M and Ramamoorthy A, *Chem. Commun.*, 2018, 54, 2000–2003.
67. Stine WB, Jungbauer L, Yu C and Ladu MJ, *Methods Mol. Biol.*, 2011, 670, 13–32. [PubMed: 20967580]
68. Fa M, Orozco IJ, Francis YI, Saeed F, Gong Y and Arancio O, *J. Vis. Exp.*, 2010, 1884. [PubMed: 20644518]
69. Vivekanandan S, Brender JR, Lee SY and Ramamoorthy A, *Biochem. Biophys. Res. Commun.*, 2011, 411, 312–316. [PubMed: 21726530]
70. Ahmed M, Davis J, Aucoin D, Sato T, Ahuja S, Aimoto S, Elliott JI, Van Nostrand WE and Smith SO, *Nat. Struct. Mol. Biol.*, 2010, 17, 561–567. [PubMed: 20383142]
71. Chimon S, Shaibat MA, Jones CR, Calero DC, Aizezi B and Ishii Y, *Nat. Struct. Mol. Biol.*, 2007, 14, 1157–1164. [PubMed: 18059284]
72. Serra-Batiste M, Ninot-Pedrosa M, Bayoumi M, Gairi M, Maglia G and Carulla N, *Proc. Natl. Acad. Sci.*, 2016, 113, 10866–10871. [PubMed: 27621459]
73. Brown AM and Bevan DR, *Biophys. J.*, 2016, 111, 937–949. [PubMed: 27602722]
74. Sahoo BR, Genjo T, Cox SJ, Stoddard AK, Anantharamaiah GM, Fierke C and Ramamoorthy A, *J. Mol. Biol.*, 2018, 430, 4230–4244. [PubMed: 30170005]
75. Straub JE and Thirumalai D, *Curr. Opin. Struct. Biol.*, 2010, 20, 187–195. [PubMed: 20106655]
76. Urbanc B, Cruz L, Ding F, Sammond D, Khare S, Buldyrev SV, Stanley HE and Dokholyan NV, *Biophys. J.*, 2004, 87, 2310–2321. [PubMed: 15454432]
77. Wei G, Mousseau N and Derreumaux P, *Prion*, 2007, 1, 3–8. [PubMed: 19164927]
78. Yang T, Li S, Xu H, Walsh DM and Selkoe DJ, *J. Neurosci.*, 2017, 37, 152–163. [PubMed: 28053038]
79. Loquet A, El Mammeri N, Stanek J, Berbon M, Bardiaux B, Pintacuda G and Habenstein B, *Methods*, 2018, 138–139, 26–38.
80. Colvin MT, Silvers R, Ni QZ, Can TV, Sergeyev I, Rosay M, Donovan KJ, Michael B, Wall J, Linse S and Griffin RG, *J. Am. Chem. Soc.*, 2016, 138, 9663–9674. [PubMed: 27355699]
81. Wälti MA, Ravotti F, Arai H, Glabe CG, Wall JS, Böckmann A, Güntert P, Meier BH and Riek R, *Proc. Natl. Acad. Sci.*, 2016, 113, E4976–E4984. [PubMed: 27469165]
82. Bertini I, Gonnelli L, Luchinat C, Mao J and Nesi A, *J. Am. Chem. Soc.*, 2011, 133, 16013–16022. [PubMed: 21882806]
83. Niu Z, Zhao W, Zhang Z, Xiao F, Tang X and Yang J, *Angew. Chemie - Int. Ed.*, 2014, 53, 9294–9297.

84. Morris KL and Serpell LC, *Methods Mol. Biol.*, 2012, 849, 121–135. [PubMed: 22528087]
85. Eisenberg D and Jucker M, *Cell*, 2012, 148, 1188–1203. [PubMed: 22424229]
86. Gremer L, Schölzel D, Schenk C, Reinartz E, Labahn J, Ravelli RBG, Tusche M, Lopez-iglesias C, Hoyer W, Heise H, Willbold D and Schröder GF, *Science* (80-.), 2017, 358, 116–119.
87. Schmidt M, Rohou A, Lasker K, Yadav JK, Schiene-Fischer C, Fändrich M and Grigorieff N, *Proc. Natl. Acad. Sci.*, 2015, 112, 11858–11863. [PubMed: 26351699]
88. Esparza TJ, Wildburger NC, Jiang H, Gangolli M, Cairns NJ, Bateman RJ and Brody DL, *Sci. Rep.*, 2016, 6, 1–16. [PubMed: 28442746]
89. Sehlin D, Englund H, Simu B, Karlsson M, Ingelsson M, Nikolajeff F, Lannfelt L and Pettersson FE, *PLoS One*, 2012, 7, e32014. [PubMed: 22355408]
90. Rostagno A and Ghiso J, *Curr. Protoc. Cell Biol.*, 2009.
91. Lesné S, Ming TK, Kotilinek L, Kaye R, Glabe CG, Yang A, Gallagher M and Ashe KH, *Nature*, 2006, 440, 352–357. [PubMed: 16541076]
92. Townsend M, Shankar GM, Mehta T, Walsh DM and Selkoe DJ, *J. Physiol.*, 2006, 572, 477–492. [PubMed: 16469784]
93. Shankar GM, Li S, Mehta TH, Garcia-Munoz A, Shepardson NE, Smith I, Brett FM, Farrell MA, Rowan MJ, Lemere CA, Regan CM, Walsh DM, Sabatini BL and Selkoe DJ, *Nat. Med.*, 2008, 14, 837–842. [PubMed: 18568035]
94. Massi F and Straub JE, in *Proteins: Structure, Function and Genetics*, 2001, vol. 42, pp. 217–229.
95. Nguyen PH, Li MS, Stock G, Straub JE and Thirumalai D, *Proc. Natl. Acad. Sci.*, 2007, 104, 111–116. [PubMed: 17190811]
96. Reddy G, Straub JE and Thirumalai D, *Proc. Natl. Acad. Sci.*, 2009, 106, 11948–11953. [PubMed: 19581575]
97. Tarus B, Straub JE and Thirumalai D, *J. Mol. Biol.*, 2005, 345, 1141–1156. [PubMed: 15644211]
98. Massi F and Straub JE, *Biophys. J.*, 2001, 81, 697–709. [PubMed: 11463618]
99. Reddy G, Straub JE and Thirumalai D, *J. Phys. Chem. B*, 2009, 113, 1162–1172. [PubMed: 19125574]
100. Rodriguez RA, Chen LY, Plascencia-Villa G and Perry G, *Biochem. Biophys. Res. Commun.*, 2017, 487, 444–449. [PubMed: 28427941]
101. Wolff M, Zhang-Haagen B, Decker C, Barz B, Schneider M, Biehl R, Radulescu A, Strodel B, Willbold D and Nagel-Steger L, *Sci. Rep.*, 2017, 7, 2493. [PubMed: 28559586]
102. Masman MF, Eisel ULM, Csizmadia IG, Penke B, Enriz RD, Marrink SJ and Luiten PGM, *J. Phys. Chem. B*, 2009, 113, 11710–11719. [PubMed: 19645414]
103. Kotler SA, Brender JR, Vivekanandan S, Suzuki Y, Yamamoto K, Monette M, Krishnamoorthy J, Walsh P, Cauble M, Holl MMB, Marsh ENG and Ramamoorthy A, *Sci. Rep.*, 2015, 5, 11811. [PubMed: 26138908]
104. Bertini I, Gallo G, Korsak M, Luchinat C, Mao J and Ravera E, *ChemBioChem*, 2013, 14, 1891–1897. [PubMed: 23821412]
105. Bellomo G, Bologna S, Gonnelli L, Ravera E, Fragai M, Lelli M and Luchinat C, *Chem. Commun.*, 2018, 54, 7601–7604.
106. Bennett AE, Ok JH, Griffin RG and Vega S, *J. Chem. Phys.*, 1992, 96, 8624–8627.
107. Rezaei-Ghaleh N, Giller K, Becker S and Zweckstetter M, *Biophys. J.*, 2011, 101, 1202–1211. [PubMed: 21889458]
108. Makin S, *Nature*, 2018, 559, S4–S7. [PubMed: 30046080]
109. Hyung SJ, DeToma AS, Brender JR, Lee S, Vivekanandan S, Kochi A, Choi JS, Ramamoorthy A, Ruotolo BT and Lim MH, *Proc Natl Acad Sci U S A*, 2013, 110, 3743–3748. [PubMed: 23426629]
110. Singh Y, Sharpe PC, Hoang HN, Lucke AJ, McDowall AW, Bottomley SP and Fairlie DP, *Chem. - A Eur. J.*, 2011, 17, 151–160.
111. Watson AA, Fairlie DP and Craik DJ, *Biochemistry*, 1998, 37, 12700–12706. [PubMed: 9737846]
112. Zheng W, Tsai M-Y, Chen M and Wolynes PG, *Proc. Natl. Acad. Sci.*, 2016, 113, 11835–11840. [PubMed: 27698130]

113. Bossis F and Palese LL, *Biochim. Biophys. Acta - Proteins Proteomics*, 2013, 1834, 2486–2493.
114. Danielson MA and Falke JJ, *Annu. Rev. Biophys. Biomol. Struct*, 2003, 25, 163–195.
115. Suzuki Y, Brender JR, Soper MT, Krishnamoorthy J, Zhou YL, Ruotolo BT, Kotov NA, Ramamoorthy A and Marsh ENG, *Biochemistry*, 2013, 52, 1903–1912. [PubMed: 23445400]
116. Brender JR, Ghosh A, Kotler SA, Krishnamoorthy J, Bera S and Morris V, 2019, 1, 4483–4486.
117. Schanda P and Brutscher B, *J. Am. Chem. Soc.*, 2005, 127, 8014–8015. [PubMed: 15926816]
118. Pradhan K, Das G, Mondal P, Khan J, Barman S and Ghosh S, *ACS Chem. Neurosci*, 2018, 9, 2929–2940. [PubMed: 30036464]
119. Ghanta J, Shen CL, Kiessling LL and Murphy RM, *J. Biol. Chem.*, 1996, 271, 29525–29528. [PubMed: 8939877]
120. Pallitto MM, Ghanta J, Heinzelman P, Kiessling LL and Murphy RM, *Biochemistry*, 1999, 38, 3570–3578. [PubMed: 10090743]
121. Biswas A, Kurkute P, Jana B, Laskar A and Ghosh S, *Chem. Commun*, 2014, 50, 2604–2607.
122. Nascia-Labouze J, Nguyen PH, Sterpone F, Berthoumieu O, Buchete NV, Coté S, De Simone A, Doig AJ, Faller P, Garcia A, Laio A, Li MS, Melchionna S, Mousseau N, Mu Y, Paravastu A, Pasquali S, Rosenman DJ, Strodel B, Tarus B, Viles JH, Zhang T, Wang C and Derreumaux P, *Chem. Rev.*, 2015.
123. Straub JE and Thirumalai D, *Annu. Rev. Phys. Chem.*, 2011, 62, 437–463. [PubMed: 21219143]
124. Massi F and Straub JE, *Protein Sci.*, 2002, 11, 1639–1647. [PubMed: 12070316]
125. Urbanc B, Cruz L, Yun S, Buldyrev SV, Bitan G, Teplow DB and Stanley HE, *Proc. Natl. Acad. Sci. U. S. A.*, 2004, 101, 17345–17350. [PubMed: 15583128]
126. Gu L, Liu C and Guo Z, *J. Biol. Chem.*, 2013, 288, 18673–18683. [PubMed: 23687299]
127. Gu L, Liu C, Stroud JC, Ngo S, Jiang L and Guo Z, *J. Biol. Chem.*, 2014, 289, 27300–27313. [PubMed: 25118290]
128. Huang D, Zimmerman MI, Martin PK, Nix AJ, Rosenberry TL and Paravastu AK, *J. Mol. Biol.*, 2015, 427, 2319–2328. [PubMed: 25889972]
129. Tay WM, Huang D, Rosenberry TL and Paravastu AK, *J. Mol. Biol.*, 2013, 425, 2494–2508. [PubMed: 23583777]
130. Spencer RK, Li H and Nowick JS, *J. Am. Chem. Soc.*, 2014, 136, 5595–5598. [PubMed: 24669800]
131. Ngo S and Guo Z, *Biochem. Biophys. Res. Commun.*, 2011, 414, 512–516. [PubMed: 21986527]
132. Zheng X, Wu C, Liu D, Li H, Bitan G, Shea JE and Bowers MT, *J. Phys. Chem. B*, 2016, 120, 1615–1623. [PubMed: 26439281]
133. Lu J, Cao Q, Wang C, Zheng J, Luo F, Xie J, Li Y, Ma X, He L, Eisenberg D, Nowick J, Jiang L and Li D, *Front. Mol. Neurosci.*, 2019, 12, 1–10. [PubMed: 30809121]
134. Hassan A, Quinn CM, Struppe J, Sergeyev IV, Zhang C, Guo C, Runge B, Theint T, Dao HH, Jaroniec CP, Berbon M, Lends A, Habenstein B, Loquet A, Kuemmerle R, Perrone B, Gronenborn AM and Polenova T, *J. Magn. Reson.*, 2020, 311, 106680. [PubMed: 31951864]

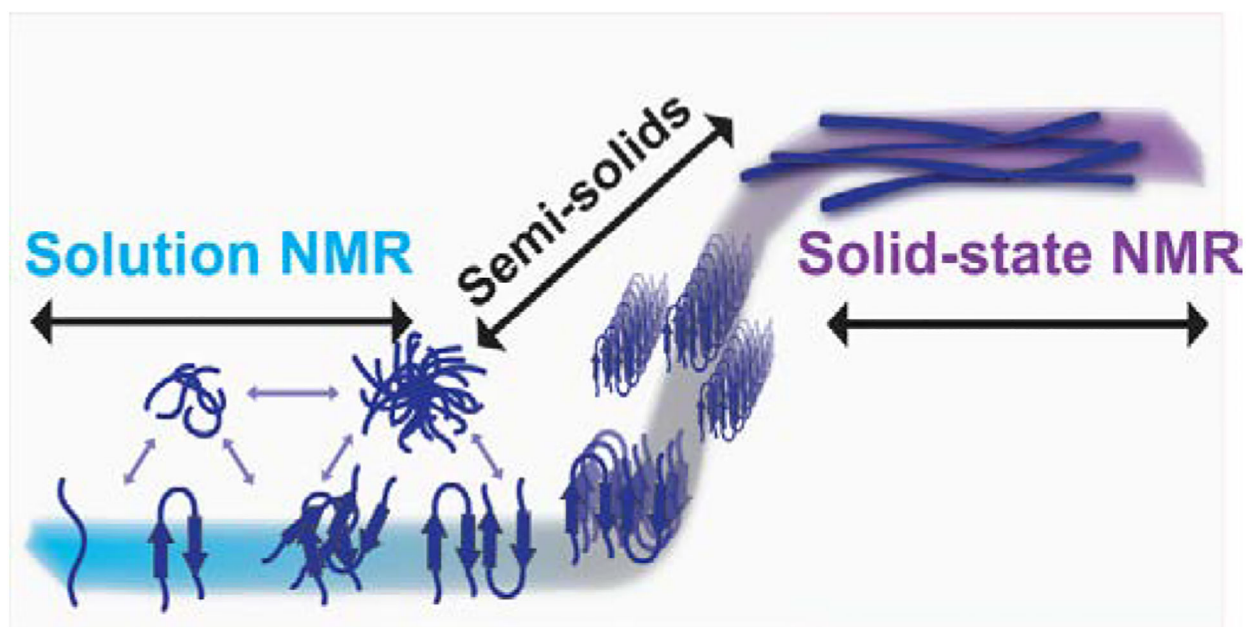
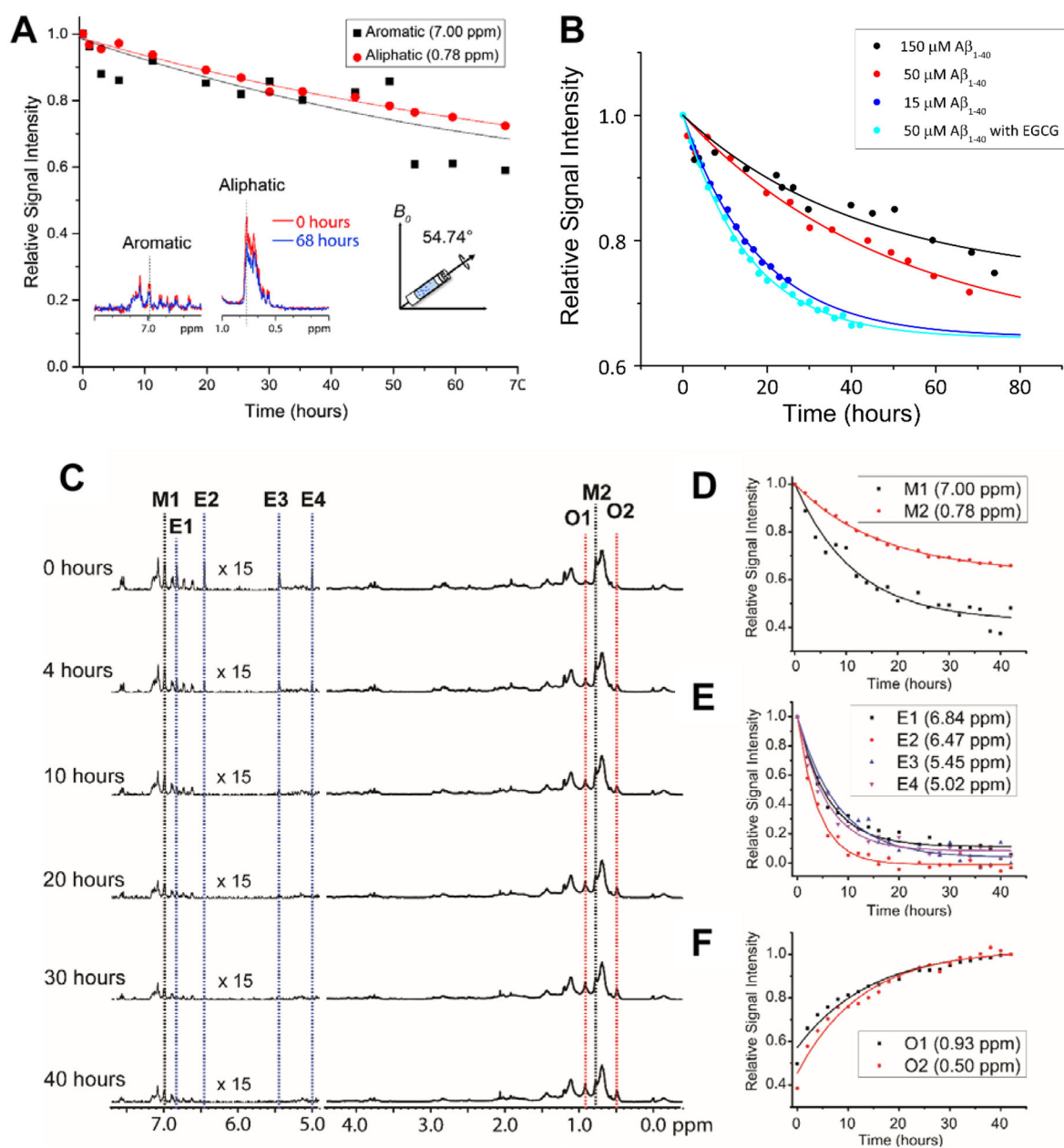


Fig. 1. Detection of amyloid species by NMR.

Solution NMR spectroscopy is well suited for high-resolution structural and dynamical studies of fast tumbling monomers and small molecular weight amyloid species like oligomers formed in the early lag phase (blue). On the other hand, magic-angle spinning (MAS) solid-state NMR techniques can be used to investigate the high-resolution structures of anisotropic, larger aggregates such as large oligomers, protofibrils and fibers (purple). In addition, as discussed in the main text, semi-solids that are not isotropic such as small to large size oligomers can also be investigated using high-resolution magic angle spinning (HR-MAS) experiments. Use of a combination of solution and solid-state NMR experiments and peptides judiciously labelled with isotopes (^{13}C , ^{15}N , ^2H , ^{19}F or a combination of them) can provide piercing atomic-resolution insights into the self-assembly process of amyloid aggregation, the formation of toxic oligomers, polymorphism of fibers and the dynamic exchange among the different species.

**Fig. 2.**

Effect of MAS on the aggregation kinetics of $\text{A}\beta_{1-40}$. **(A)** Depletion in $\text{A}\beta_{1-40}$ monomer population under MAS (5 kHz MAS at 298K) as indicated by the decay of ^1H NMR signal intensity for selected aliphatic and aromatic resonances of freshly prepared 50 μM $\text{A}\beta_{1-40}$ as a function of time (time=0 refers the data acquired in <10 minutes from the sample preparation). **(B)** Relative ^1H NMR signal intensity decay of methyl resonance (0.78 ppm) under 5 kHz MAS as a function of $\text{A}\beta_{1-40}$ monomer concentration in the absence or presence of EGCG. The curves were fitted using the equation $y=(1-A)*\exp(-b*x)+A$, where A is the proportion that remains as monomer after saturation and b is the rate of decay or aggregation. **(C)** The polyphenolic EGCG compound promotes $\text{A}\beta_{1-40}$ aggregation (50 μM) under MAS (under 5 kHz MAS and 298K) as observed from the decay of ^1H NMR signal as

a function of time. **(D–F)** The aromatic ^1H signals decay faster as compared to aliphatic protons in $\text{A}\beta_{1-40}$ (50 μM) in the presence of EGCG indicating the role of predominant π - π interactions. The aromatic proton signals of EGCG also show a rapid depletion in intensity **(D)** indicating a strong interaction with $\text{A}\beta_{1-40}$. **(E)** The appearance of new peaks O1 and O2 indicates the formation of new oligomer species. An increase in the oligomer populations over time is revealed by an increasing ^1H signal intensities O1 and O2 species. This figure is reproduced with permission from the Royal Society of Chemistry (<https://doi.org/10.1039/C8CC00167G>). Further details can be found in the referenced work.⁵¹

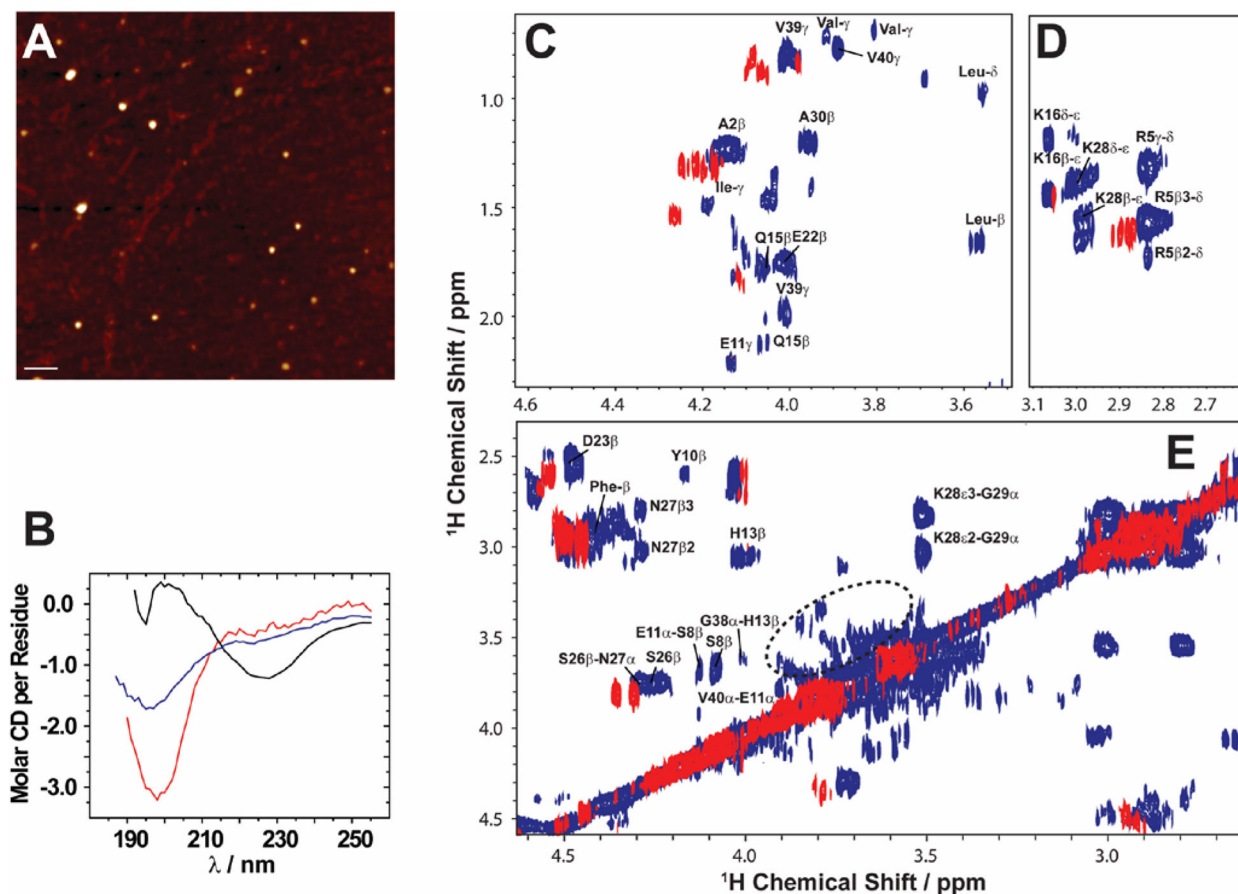


Fig. 3. Solid state NMR allows characterization of growing low abundance Aβ₁₋₄₀ oligomers. (A) AFM image showing the presence of Aβ₁₋₄₀ oligomers (left) after separation from fibers after 4 days (scale bar is 100 nm). (B) CD spectra show that the filtered Aβ₁₋₄₀ oligomers (blue) are disordered, similar to the freshly dissolved monomers (red), and differ from the β-sheet rich fibers (black). (C–E) 2D ¹H/¹H NMR spectra obtained via RFDR recoupling of ¹H-¹H dipolar couplings show high-resolution cross-peaks for oligomers (blue) and freshly dissolved Aβ₁₋₄₀ monomers (red); spectra recorded at 25 °C under 2.7 kHz MAS on a 600 MHz solid-state NMR spectrometer. The spectrum highlights the observation of cross-peaks due to the recoupled ¹H-¹H dipolar couplings for (C) side-chain to Hα, (D) side-chain, and (E) Hβ-Hα and Hα-Hα regions. The acquisition time was 4 days. The 2.7 kHz MAS and RFDR mixing enabled the suppression of signals from monomers and fibers and selective observation of low molecular weight oligomers in a non-perturbative manner. The NMR samples were prepared in 10 mM phosphate buffer, pH 7.4, and 10% D₂O. Copyright © 2015, Springer Nature. This figure is reproduced from Scientific Reports: <https://doi.org/10.1038/srep11811>. Further details can be found in the referenced work.¹⁰³

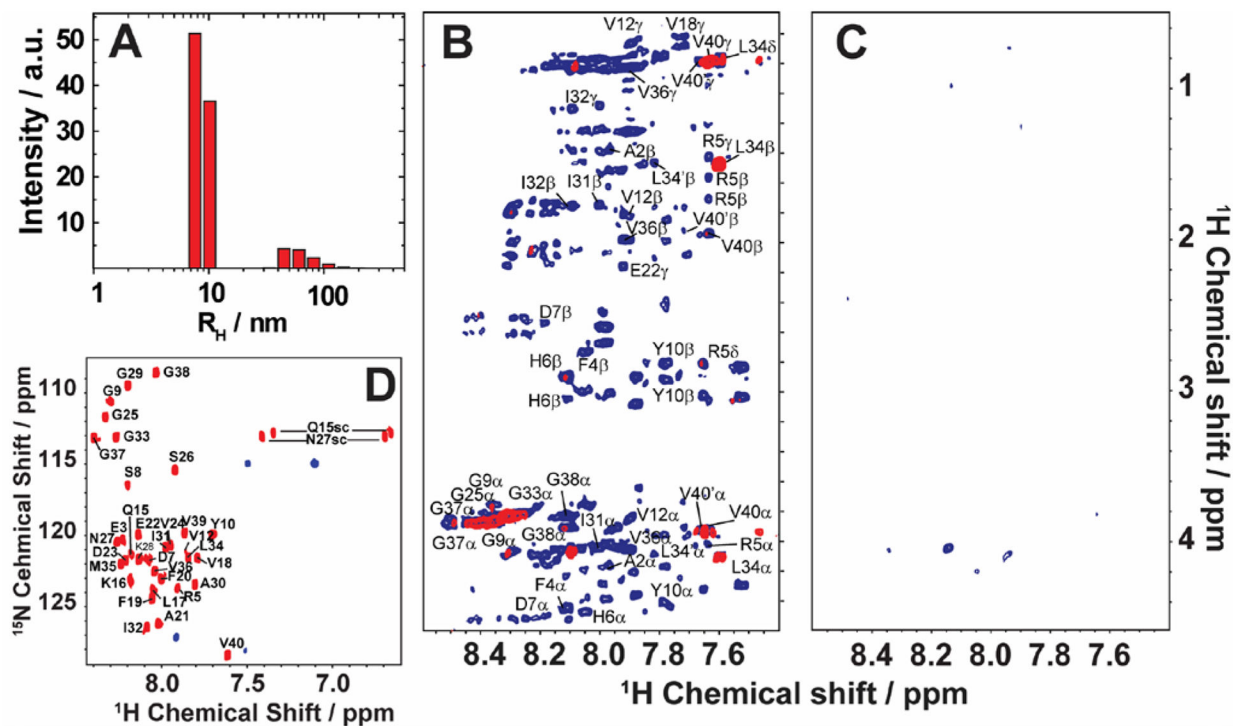


Fig. 4.

Monitoring time-lapse growth of Aβ₁₋₄₀ oligomers by NMR. (A) Dynamic light scattering reveals the growth of Aβ₁₋₄₀ oligomers from 8.6 nm and 65.3 nm over the course of 19 days. 2D TOCSY (B) and 2D NOESY (C) spectra of the disordered Aβ₁₋₄₀ oligomers recorded at 4 days (blue) and 19 days (red). Both TOCSY and NOESY spectra show line-broadening on day-19 indicating the growth of oligomer size that are beyond the detection limit of solution NMR. (D) 2D $^1H/^{15}N$ HSQC spectra of the freshly dissolved (red) Aβ₁₋₄₀ recorded on a 900 MHz NMR spectrometer show well resolved NMR peaks. In contrast, $^1H/^{15}N$ HSQC spectra of the filtered disordered oligomers (blue) obtained after 4 days show substantial line broadening. The NMR samples were prepared in 10 mM phosphate buffer, pH 7.4, and 10% D₂O and NMR spectra were recorded at 25 °C. Copyright © 2015, Springer Nature. This figure is reproduced from Scientific Reports: <https://doi.org/10.1038/srep11811>. Further details can be found in the referenced study.¹⁰³

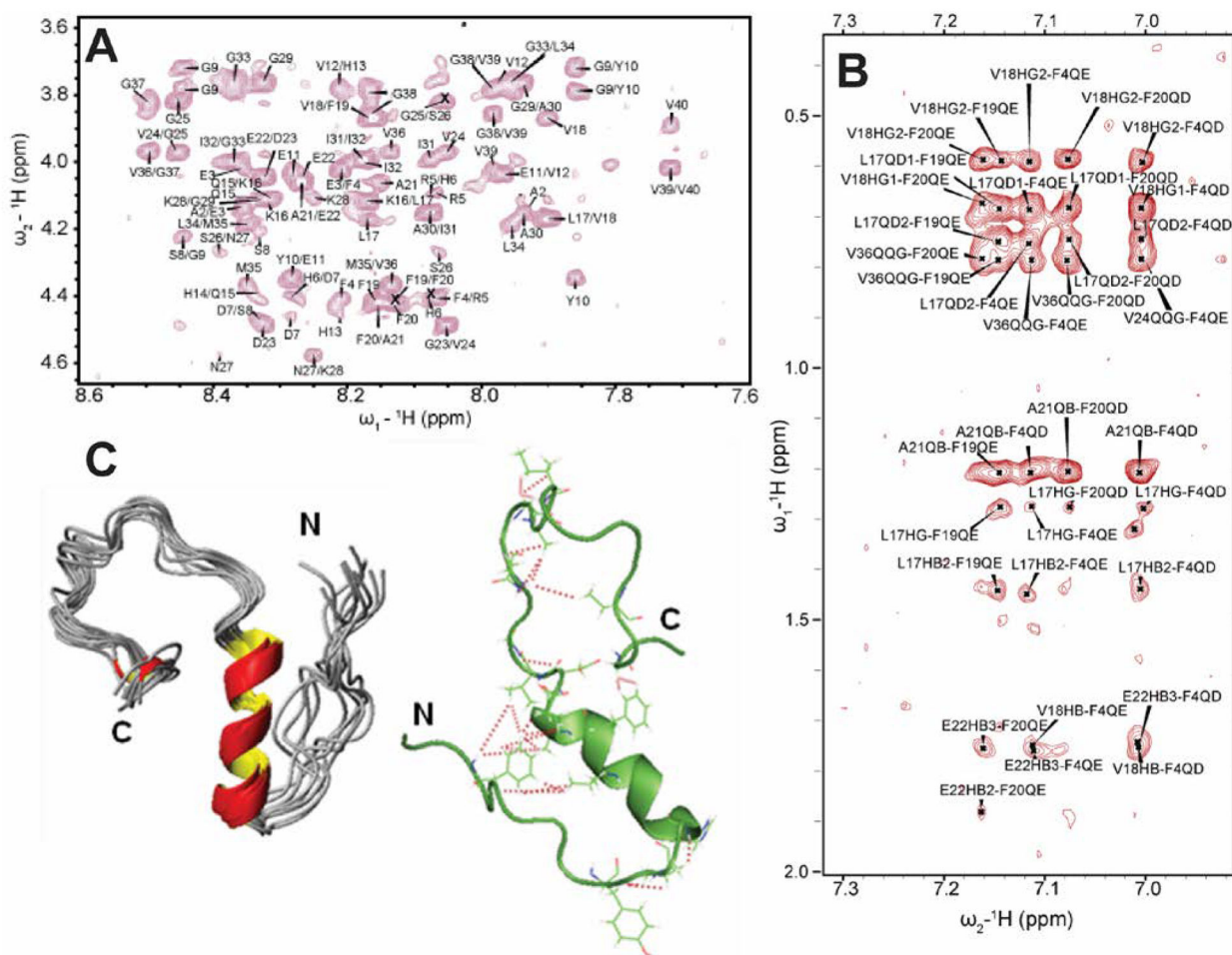


Fig. 5. 3D structure of a small molecular weight $\text{A}\beta_{1-40}$ oligomer determined by solution NMR. (A) 2D NOESY spectrum of 77 μM $\text{A}\beta_{1-40}$ dissolved in 20 mM potassium phosphate, 50 mM NaCl, pH 7.3 containing 93% H_2O and 7% D_2O recorded at 15 $^\circ\text{C}$ on a 900 MHz NMR spectrometer. The selected regions show NOEs that corresponds to the sequential assignment of $\text{H}_{\alpha i}-\text{N}_{\text{Hi}+1}$. (B) The aromatic region of the NOESY spectrum showing cross-peaks between F19 and F20 residues, the C-terminus and F4 residue, and the central helical region of the peptide. (C) 3D NMR structures of $\text{A}\beta_{1-40}$ calculated from NOEs and backbone dihedral angle restraints. The cartoon structure shown on the right in green shows the long-range NOEs that stabilizes the formation of the hairpin structure and the bends in the N- and C-termini (red dashed lines). Copyright © 2011 Elsevier Inc. This figure is reproduced with permission from Biochemical and Biophysical Research Communications: <https://doi.org/10.1016/j.bbrc.2011.06.133>. Further details can be found in the published article.⁶⁹

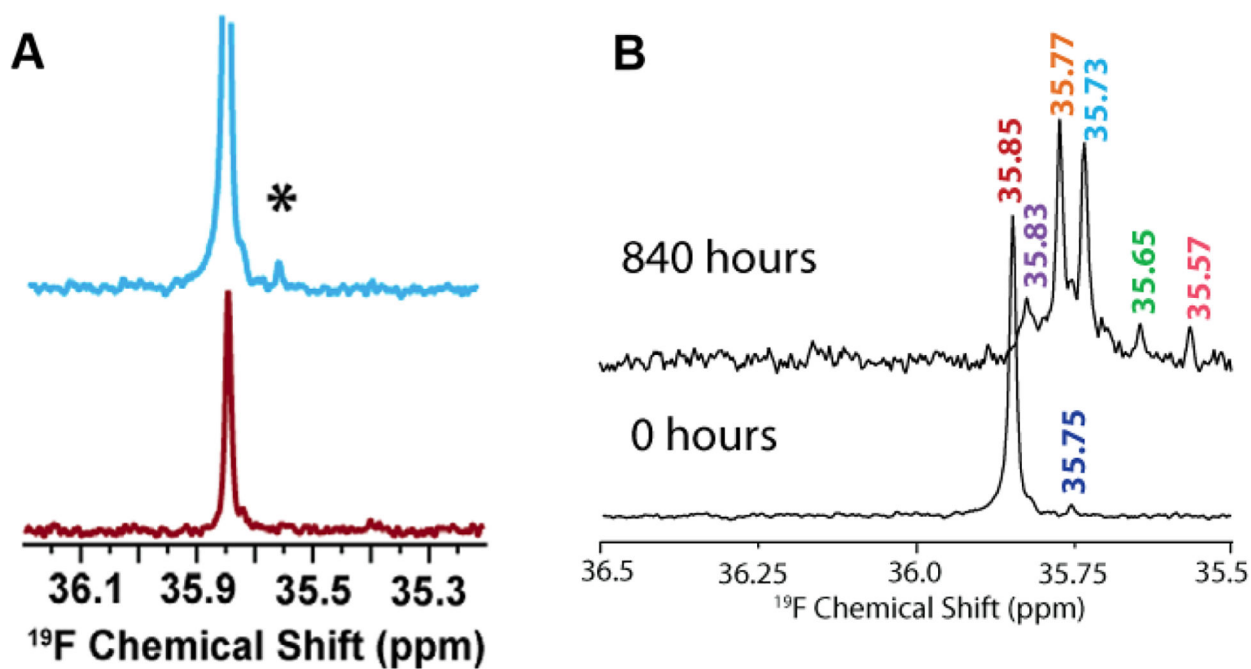


Fig. 6.

(A) Characterization of $\text{A}\beta_{1-40}$ oligomers using ^{19}F NMR. Fluorinated $\text{A}\beta_{1-40}\text{-tfM}_{35}$ showing the presence of an additional peak (denoted as *) for a freshly prepared 182 μM peptide sample (blue) as compared to 46 μM sample (red). The small additional peak indicates $\text{A}\beta_{1-40}\text{-tfM}_{35}$ oligomerization. The intensities of both samples are normalized to an internal TFE standard. (B) Monitoring the aggregation behavior of 182 μM $\text{A}\beta_{1-40}\text{-tfM}_{35}$ by ^{19}F NMR at two different time intervals. The appearance of multiple peaks at 840 hours indicates the presence of variable sized $\text{A}\beta_{1-40}\text{-tfM}_{35}$ species. Copyright © 2013, American Chemical Society. This figure is reproduced with permission from [dx.doi.org/10.1021/bi400027y](https://doi.org/10.1021/bi400027y); *Biochemistry* 2013, 52, 1903–1912. Further details can be found in the published study.¹¹⁵

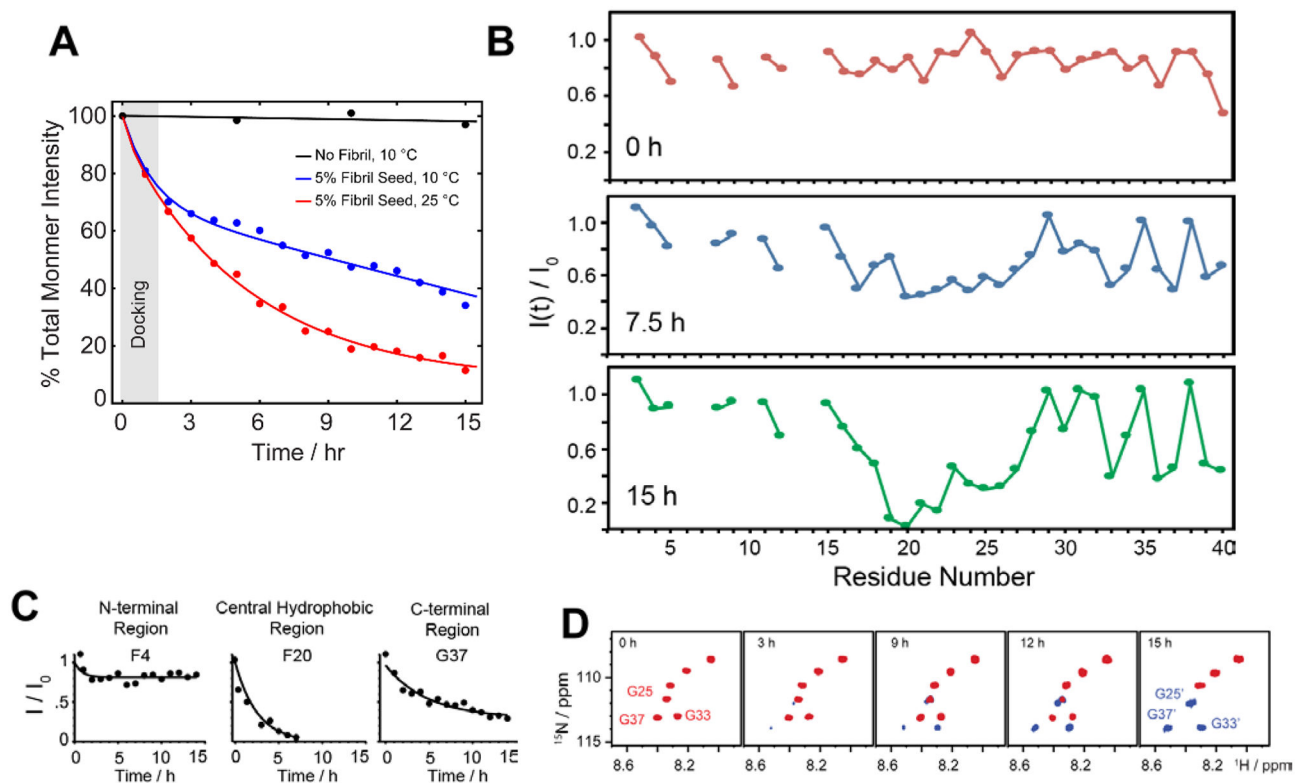


Fig. 7. Probing dock-lock mechanism in $A\beta_{1-40}$ by solution NMR.

(A) Monitoring the depletion of total intensity obtained from 2D ^1H - ^{15}N SOFAST-HMQC spectra during a self-seeding reaction at 10 °C. The observed distinguished kinetic phase (black vs blue curve) indicates the dominant docking phase (grey shade) within a time-scale of first couple of hours. (B–C) Time-interval measurement highlights a substantial drop in NMR signal intensities of the central hydrophobic residues (F20 as a representative residue) as compared to N- or C-terminal residues (F4 and G37 as representative residues) indicating a possible docking site in monomer onto fully matured fibers. (D) NMR self-seeding reaction identified appearance of new peaks in the SOFAST-HMQC spectrum indicating the origin of new oligomer species. Copyright © 2019 Royal Society of Chemistry. Reproduced by permission from the Royal Society of Chemistry <https://doi.org/10.1039/C9CC01067J>. Further details are available in the referenced work.¹¹⁶